Heat Capacity, Thermal Expansion Coefficient, and Grüneisen Parameter of CH_4, CO_2 and C_2H_6 Hydrates and Ice I_h via Density Functional Theory and Phonon Calculations

*Samuel L. Mathews, Phillip D. Servio, Alejandro D. Rey**

Department of Chemical Engineering, McGill University, Montreal, Quebec H3A 0C5, Canada

ABSTRACT. Thermal properties of gas hydrates and its underlying fundamental characterization are limited and incomplete but crucial in on-going basic science research and technological applications. The constant volume heat capacity, the constant pressure heat capacity, the volumetric thermal expansion coefficient, and the Grüneisen parameter of methane, ethane, ethylene oxide, carbon dioxide, and empty sI hydrates, and of hexagonal ice, as functions of temperature from 0 to 300 Kelvin were calculated using the integration of DFT simulations at 0K and phonon calculations at higher temperatures. At low temperatures, DFT predictions replicated experimental values of constant pressure heat capacity for hydrates and ice accurately. Notably the constant volume heat capacity was lower than when compared with literature values calculated with MD, and closer to actual data. Guest molecules were found to contribute slightly more than their ideal gas heat capacities to the overall property of the system. DFT underestimated the thermal expansion coefficient in all cases. The ethane and carbon dioxide hydrates demonstrated behavior that was markedly different when compared to methane and empty hydrates, and hexagonal ice. The Grüneisen parameter was calculated for all systems. DFT overestimated the value of the parameter for filled hydrates and hexagonal ice when compared to experimental hexagonal ice values. Altogether, this systematic atomistic study contributes to the technological applications and basic material science of these crystals whose properties are of significant importance in the fields of energy and the environment and provides a potential input to MD simulations thanks to its performance at low temperatures.

INTRODUCTION

Gas hydrates are a class of clathrates formed by water molecules hydrogen bonded into a crystalline network of cages. Since the backbone is formed by water, gas hydrates are often compared to hexagonal ice[1]. Unlike ice, water molecules interact via hydrogen bonds and enclose a gas molecule. There exist three main structures of gas hydrates, structure I (sI), structure II (sII), and structure H (sH). Gas hydrates are present around the world in various industries. In natural gas extraction, water is always present in natural gas reservoirs. Additionally, it is often used to remove carbon dioxide and hydrogen sulfide, "acid gases" present in the natural gas. Therefore, hydrates will be encountered throughout natural gas production[1], where they are considered a problem. Gas hydrates can also be used in gas separation, desalination, gas storage, and carbon dioxide sequestration due to their unique structural packing[2]. Gas hydrates are also considered a large, global energy source. Enormous reserves are present under continental shelves across the world and the total amount of carbon in these reserves is estimates to nearly double the amount of carbon in all other fossil fuel reserves combined. Because cost, environmental concern, and resource availability all favor the use of natural gas, a common guest in hydrates, the exploitation of these reserves is becoming more important and necessary. To exploit them in a safe and effective manner, studying and prediction their properties has become essential[3]. Various properties are involved in various methods of natural gas hydrate exploitation, and these methods vary by location of the deposit[4,5].

The thermal properties considered in this paper are of crucial importance in equilibrium conditions, phase transitions during decomposition and formation, as in crystal growth and melting. Obtaining hydrate thermal properties is costly due to pressure conditions and often complicated because the properties depend on the cage occupancy, the guest molecule, and the structure of the hydrate[1]. The physical, chemical, and interfacial properties of sI and sII have been historically studied first, while sH is still lacking the same quality and quantity of data[6–13]. This arises because sH is not commonly seen in natural gas hydrate studies. However, it is becoming a structure of interest in other applications, such as gas storage[9,14]. Due to difficulties in preparing and measuring properties of hydrates in the laboratory and comparing those properties to simulations, notable discrepancies in thermal properties exist even for the same hydrates[10,13,15].

The thermal properties of gas hydrates have been previously studied theoretically using molecular dynamics. One study[16] found that the results for thermal properties varied with estimation techniques and the omission or inclusion of long-range electrostatics. Another molecular dynamics study[13] found some difference between guest molecules, but large differences with experiment. Ab initio molecular dynamics has also been used to calculate thermal properties. One study[17] using this technique calculated the constant volume and pressure specific heats, as well the thermal expansion coefficient of the methane hydrate. The calculated thermal expansion coefficient was almost 40% lower than another study[18] which calculated the same property using molecular dynamics, and higher than ice.

In this work, we compute the constant volume heat capacity, the constant pressure heat capacity, the thermal expansion coefficient, and the Grüneisen Parameter of methane, ethane, carbon dioxide, and empty sI hydrates, and of hexagonal ice, as functions of temperature from 0 Kelvin to 300 Kelvin, to examine the similarities between the hydrate structures and ice, while providing insights into the influence of different guest molecules on the properties due to their chemistry and geometry. As a part of this objective, this work simulates the atomic configurations in the zero-Kelvin environment of ab initio density functional theory (DFT) to explain and examine macroscopic, real-temperature behavior using atomic-scale information and fundamental thermodynamics implemented in phonon calculations.

The organization of this paper is as follows. The methodology will present the techniques used for the computations, starting with general computational details that were used for the force/energy calculations, followed by an explanation of the technique used for the calculation of the thermal properties. Then, the results are presented, along with other experimental and theoretical data for comparison.

METHODOLOGY

General Computational Details. Our computations were performed using first-principles density functional theory as implemented in the Vienna Ab Initio Simulation Package (VASP) software[19–22]. The Strongly Constrained and Appropriately Normed Semilocal (SCAN) exchange-correlation (XC) functional was employed as part of the computation. At a minimum, the SCAN functional duplicated the accuracy of more expensive hybrid functionals at the cost of a generalized gradient approximation (GGA) functional[23,24]. When compared to other functionals available, the SCAN functional provided the best error cancellation for atoms and Jellium Spheres[25] and describes the water structure very well[26]. We used the modified version of the Vydrov-van Voorhis (rVV10) nonlocal correlation functional of Peng et al. to account for long range dispersion interactions[27–30]. Projector augmented wave potentials[31,32] were employed for all calculations. The plane wave energy cut off used was 520 eV, in accordance with the high accuracy mode implemented in VASP, in addition to using an augmentation grid to improve accuracy for phonon calculations[33]. The electronic energy tolerance used was 10^{-8} eV and the ionic optimization force tolerance used was 0.5 meV/Å, in accordance with our previous work[7,9,10]. We used a k-point mesh comprised of 14 irreducible k-points, ensuring proper convergence with respect to the total energy for all systems. Although DFT is a 0 Kelvin calculation, it does not employ empirically determined interatomic potentials and is often called a first-principle calculation when compared to another commonly used approach for theoretical studies of hydrates[12,13], molecular dynamics (MD)[34].

We performed simulations of a single unit cell of sI hydrate. The cell contains 46 water molecules and can accommodate eight guest molecules. Two pentagonal dodecahedral voids (small cages) and six tetrakaidekahedron voids (large cages) make up the structure[35]. The initial atomic positions of the oxygens and the hydrogens were initially obtained by Takeuchi et al.[36] The oxygen coordinates were obtained by X-ray diffraction and the proton positions by generating structures that followed the Bernal-Fowler ice rules and finding the one that had the lowest potential energy and a net dipole moment of zero. For each respective guest, the molecule was placed at the center of each of the eight cages. Then, ionic optimization was performed according to the set force tolerance for each structure individually to obtain the ground state configuration for each system. This resulted in 100% cage occupancy. The hexagonal ice structure was the traditional Bernal-Fowler hexagonal ice lattice, with its coordinates obtained from literature[37]. It was subsequently also relaxed like the other structures. Two software packages were used for visualization: VESTA[38] and OVITO[39].

Thermal Properties. The constant volume heat capacity, the constant pressure heat capacity, and the thermal expansion coefficient were calculated following the procedures outlined in the usage of Phonopy, a phonon calculation package[40] used for a variety[41–43] of thermal transport, first principles calculations. Once the relaxed, ground state atom configurations were generated, they were used as the base unit cell in the package. Atomic configuration files were generated via the finite displacement method, using an atomic displacement distance of 0.01 Å as in our previous work in spectrometry[7,44]. For the constant pressure heat capacity and thermal expansion, the thermal contribution of thermal expansion to the constant volume heat capacity was calculated by using five volume points, two below and two above the ground state configuration for a total of five volumes per system. A cubic mesh composed of 27,000 q-points was used for integrations for all calculations involving integrals over the phonon wave vectors. The supercell approach was considered but not used for the hydrate systems due to intense, order of magnitude increases in computational costs. However, for the hexagonal ice, a cubic supercell, formed by eight unit cells was used because of the small size of its base cell. The 36-atom unit cell became a 288-atom super cell, slightly higher than the 202-atom unit cell of the ethane hydrate. Additionally, the number of displacements in the hexagonal ice supercell was lower than the hydrate systems. The properties of interest were calculated from 0 Kelvin to 300 Kelvin. The mesh used for the phonon calculations was numerically converged for all systems. Phonopy allowed for the expansion of our previous work[17] to calculate the temperature dependence for a variety of guests of the heat capacities and thermal expansion by using fundamental thermodynamics and the well-known quasi-harmonic approximation (QHA).

Carefully tailoring these techniques and software allowed for the development of an efficient workflow for use in calculating thermal properties of gas hydrates. After the ground state atomistic coordinates are generated through an initial relaxation, they are used to generate configuration files corresponding to finite displacements for each atom in six different directions. Then, the energy of each system is calculated using robust but rapid algorithms. The energies and force constant are then used in Phonopy to generate the thermal properties. Using DFT as the energy and force calculator, and Phonopy as the pre- and post-processing tool, the thermal properties of a variety of gas hydrate systems may be calculated efficiently, generating large amounts of data for comparison as shown in Figure 1.

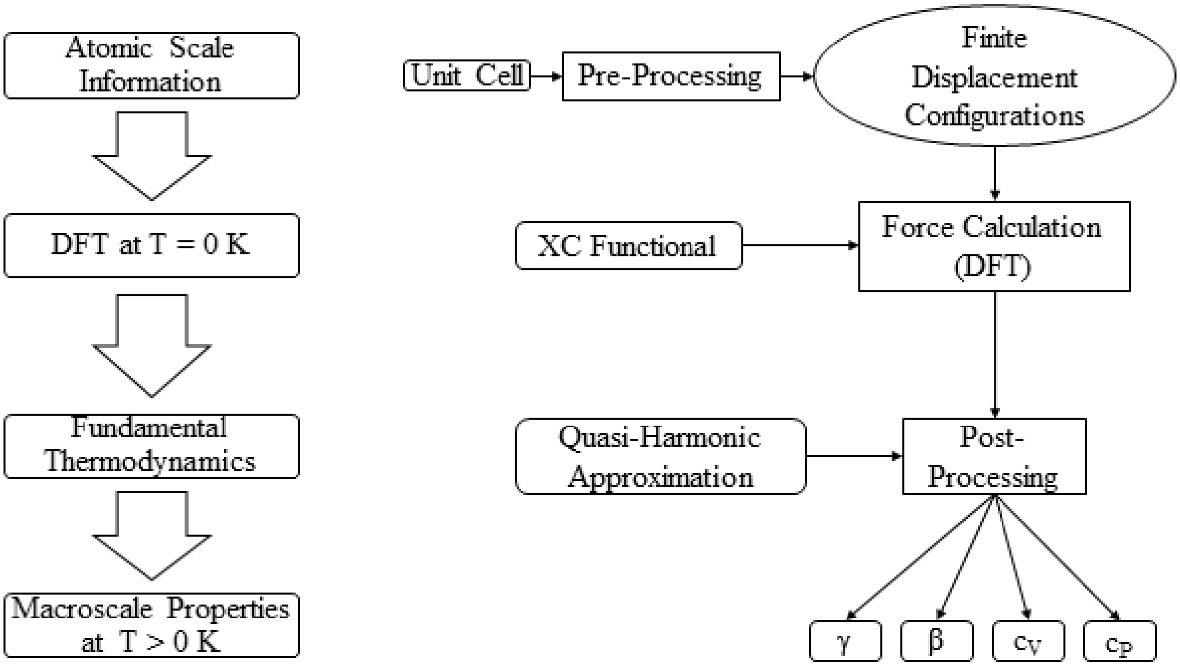

Figure 1. An overview of the process employed by this work, showing that by using atomic scale information, calculations performed at zero Kelvin through DFT can be extended through fundamental thermodynamics to properties and applications at more relevant temperatures.

RESULTS AND DISCUSSION

Constant Volume Heat Capacity. As mentioned above, we computed the constant volume heat capacity of the methane, ethane, and carbon dioxide sI hydrates, the empty sI hydrate backbone, and hexagonal ice Ih from 0-300 K at zero pressure, shown in Figure 2. Results obtained via molecular dynamics for trimethylene oxide (TMO), ethylene oxide (EO), formaldehyde (FA), cyclobutene (CB), cyclopentane (CP), and ethane (Et) sI gas hydrates are also plotted for comparison. The DFT results show similar trends regardless of guest molecule and are similar to hexagonal ice throughout the temperature range. Since this heat capacity is measured at constant volume, there is no hydrate cage expansion and if heat capacity trends are structure expansion related, the differentiation cannot be seen with constant volume heat capacity. Methane hydrates have the highest heat capacity of this type because of the ability of the methane molecule to rotate freely in the hydrate structure, an additional degree of freedom. This is confirmed by the lack of ionic optimization with regards to the methane molecule orientation in our work and by X-ray diffraction[36]. The next highest hydrate, according to DFT, is the ethane hydrate (beyond 70 Kelvin). This is because of the ability of the two methyl groups and their degrees of freedom and the restriction caused by the alignment of the ethane molecule to the hexagonal face of the $5^{12}6^{2}$ cages. The third highest structure is the empty hydrate backbone. As expected, at very low temperatures it has the smallest heat capacity and it nearly equal to ice. However, as temperature increases this behavior deviates and it falls in line with the trend of other hydrates. It is also expected that it has the lowest heat capacity out of the hydrates, except for carbon dioxide, because it possesses the least degrees of freedom by virtue of not having a guest molecule. Hexagonal ice is the closest to the hydrate backbone. Its heat capacity is lower than the backbone because it possesses less degrees of freedom in its structure, with less edges and vertices in the structure to bend and stretch. The carbon dioxide hydrate has a heat capacity equal to that of the methane hydrate before 50 Kelvin. However, it shows a decrease in its slope as temperature increases, eventually going lower than hexagonal ice at 250 Kelvin. This would indicate that the guest molecule interacts with the hydrate backbone to create a system with less degrees of freedom than the ethane hydrate and that over time it cannot vibrate, move, or rotate as freely. While carbon dioxide, being double bonded triatomic linear molecule as opposed to ethane, has less degrees of freedom, it still goes against the shown trend with the other hydrates. Since the structure affects the way molecular vibrations occur due to atomic interactions, changes in the backbone due to these interactions may increase or decrease the heat capacity.

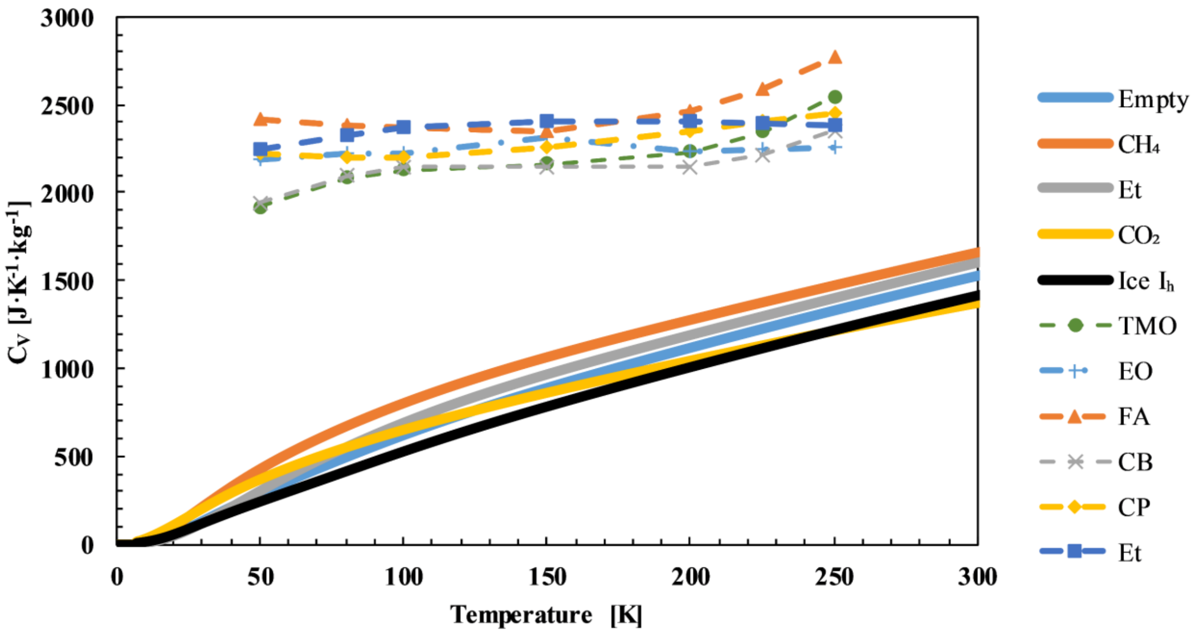

Figure 2. Temperature dependence of the constant volume heat capacity of various sI hydrate systems and hexagonal ice. The trimethylene oxide (TMO), ethylene oxide (EO), formaldehyde (FA), cyclobutene (CB), cyclopentane (CP), and ethane (Et) sI gas hydrates results are performed with MD by Ghafari et al.[13]

Molecular dynamics studies of the constant volume heat capacity are also shown in Figure 2. They were performed for guest molecules of varying polarity and structure using a cubic supercell consisting of nine sI unit cells[13]. The results of those studies produced heat capacities between 200% and 500% higher than those produced by DFT because those studies employed non-polarizable and rigid water models.[13] Additionally, the potentials and models used for the guest molecules may not appropriately describe the guest-host interactions, or do so differently when compared to DFT, which would produce large discrepancies. Also, these studies showed that the heat capacity is a much weaker function of temperature. As in our work, the MD results show overall small variations in heat capacity with guest type and electron density (for example, methane versus carbon dioxide or ethane versus ethylene oxide). Without experimental constant volume heat capacity, it is difficult to establish a preferred or more accurate methodology.

Constant Pressure Heat Capacity. In our work, we computed the constant pressure heat capacity of the methane, ethane, and carbon dioxide sI hydrates, the empty sI hydrate backbone, and hexagonal ice Ih from 0-300 K at zero pressure, shown in Figure 3. Results obtained via molecular dynamics for TMO, ethane, carbon dioxide, and methane sI gas hydrates are also plotted for comparison. Experimental results for methane and ethane sI gas hydrates, hexagonal ice, and propane (Pr) sII gas hydrates are also included and compared. Figure 3 shows very similar trends to Figure 2. DFT results show similar trends regardless of the guest molecule. Methane hydrates have the highest heat capacity because they have more degrees of freedom. The ethane hydrate is the second highest heat capacity and the carbon dioxide hydrate shows the same deviation as in the constant volume case.

When compared to Figure 2, Figure 3 is consistent with fundamental thermodynamics. The difference between the constant volume heat capacity and the constant pressure heat capacity is the thermal expansion contribution, which for solids is usually low. The difference between the two capacities is less than 5% across the range of presented temperatures and constant pressure heat capacity is always higher, consistent with fundamental thermodynamics[40]. In the constant pressure case, the ethane hydrate approaches the methane hydrate heat capacity at higher temperatures because the structure is expanding due to the temperature. This allows the ethane hydrate to move more freely compared to lower temperature states, augmenting the degrees of freedom of the ethane molecule. Once again, the hydrates have similar heat capacities to hexagonal ice. The difference lies in the containment of a guest molecule, which increases the degrees of freedom of the structure, allowing for more energy storage.

Constant pressure heat capacity can be more easily measured in the laboratory setting and Figure 3 presents experimental data for ice and methane, ethane, and propane hydrates. Experimental data shows that hydrates and ice have a similar heat capacity, and that its correlation with temperature is linear. At approximately 50 Kelvin, the DFT results deviate from the trend of experimental data and after this point, the heat capacity shows a weaker correlation with temperature. Even though the goal is to use thermodynamics to extend information obtained from the zero-Kelvin environment of DFT to real temperatures, it is important to remember that the basis is still a zero-Kelvin structure and, in this case, DFT is resolving temperature effects that have become averaged out or cancelled by other phenomena that it cannot capture.

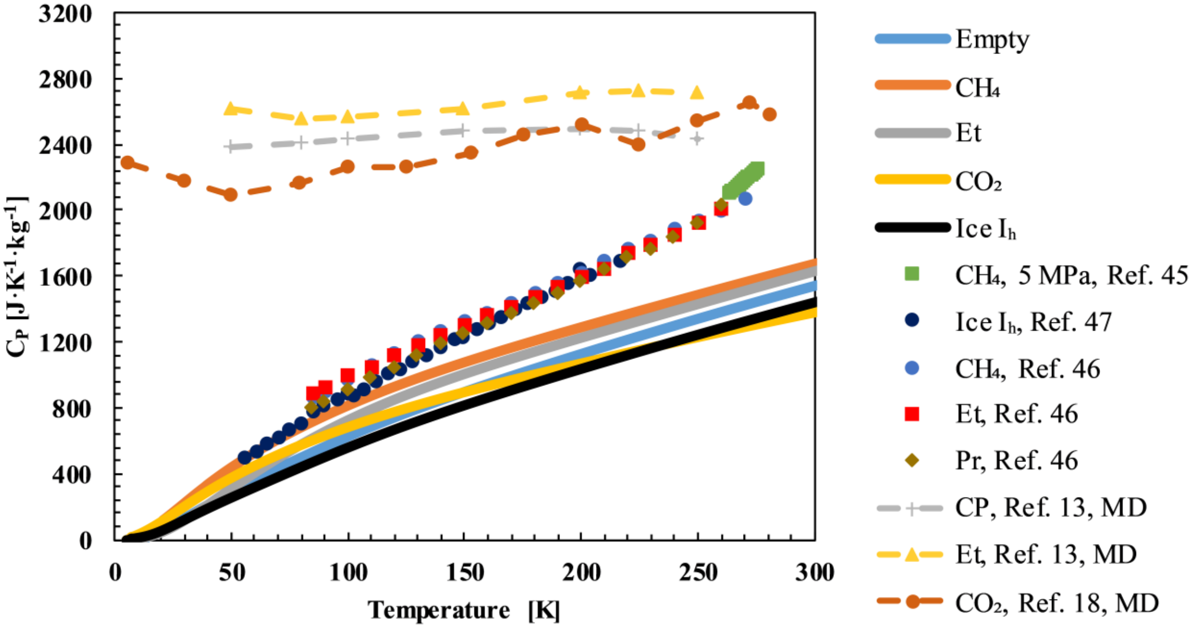

Figure 3. Temperature dependence of the constant pressure heat capacity of various sI hydrate systems and hexagonal ice. Experimental results are provided for CH_4 at 5 MPa[45] and pressures always above the dissociation pressure[46], for Et[46], Pr[46], and ice I_h[47]. The CP and Et MD results are provided by Ghafari et al.[13] The CO_2 and CH_4 MD results are provided by Ning et al.[18]

Molecular dynamics studies of the constant pressure heat capacity are also shown in Figure 3. The results of those studies produced heat capacities that 200% and 500% higher than those we produced and showed that the heat capacity is a weak function of temperature. Like this work, the molecular dynamics studies showed overall small variations in heat capacity with guest type and electron density. These studies show poor agreement with experiment across all temperatures. The correlation with temperature is much weaker and the values are overestimated. Although molecular dynamics can be stronger at higher temperatures, it does not indicate a change in trend that would allow it to replicate experimental data as well as DFT. Based on this study, it is seen that DFT paired with the QHA for phonons captures guest-host interactions better than MD. Modelling individual atoms as opposed to water or guest molecules as a single unit, as done in the two MD studies presented, allows for varied stretching and deformation of bonds or hydrate cages. Having potentials for each atom allows for a better description of guest-guest and guest-host interactions. The shortcomings of MD are present for all presented guest molecules, indicating a systematic need for improved polarizable water molecules and better H_2O and guest molecule potentials that have been fit to *ab initio* data.

As part of our work, we also computed the heat capacity gas contribution of the methane, ethane, and carbon dioxide hydrates. The contribution is taken as the difference between the heat capacity of the hydrate backbone and that containing a guest molecule. These are presented in Figure 4 along with the ideal gas heat capacities of methane, ethane, and carbon dioxide. The contribution from the methane gas should be like that of an ideal gas.[48] Data was only available to temperature down to 40 K.

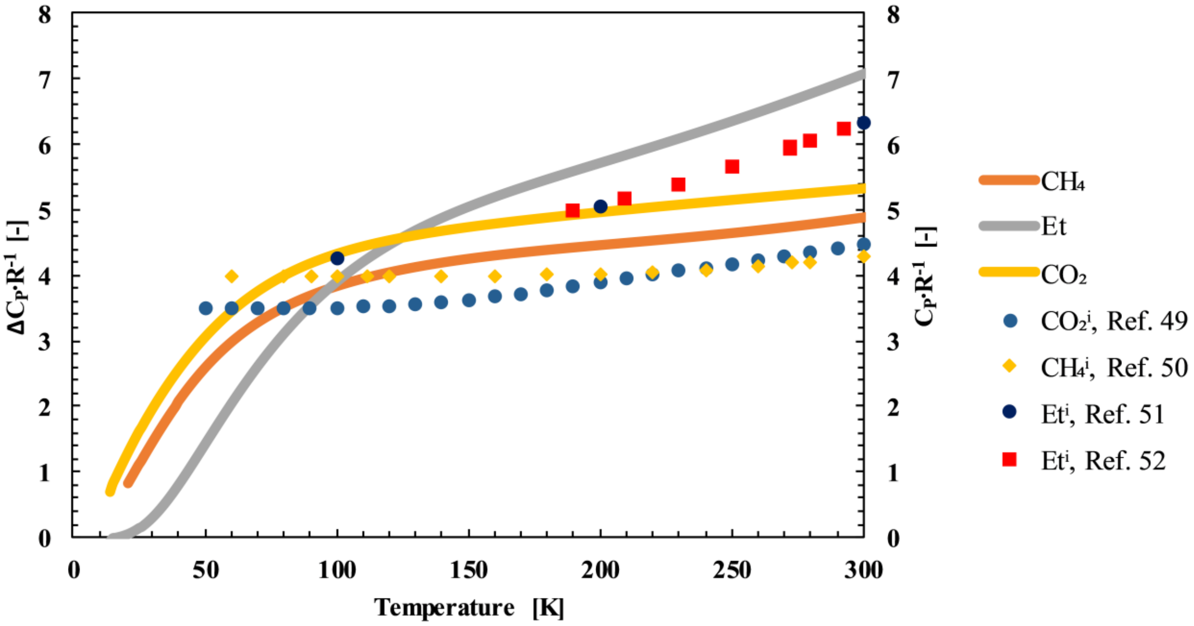

Figure 4. Temperature dependence of the heat capacity contribution, (left) normalized to the ideal gas constant compared with the ideal gas heat capacity, (right) normalized to the ideal gas constant. The DFT calculations are compared with the ideal gas heat capacities of carbon dioxide[49], methane[50], and ethane[51,52].

Our results overestimate the contribution for each guest molecules above 100 K. At 200 K we calculated a contribution of 4.5*R*, 5.7*R*, and 5.0*R* for methane, ethane, and carbon dioxide, respectively, where *R* is the ideal gas constant. At the same temperature, Handa[46] calculate contributions of $4R$ and $6.5R$ for methane and ethane hydrates experimentally. The ideal gas heat capacities of methane, ethane, and carbon dioxide at 200 K are $4.0R$, $5.1R$, and $3.9R$. Like Handa, we showed that the heat capacity contribution of sI gas hydrates is higher than the ideal gas heat capacity (above 100 K). The guest molecules not only bring their inherent heat capacity to the property, but they also interact with the hydrate structure to increase their contribution to the heat capacity. This is shown by our theoretical work and the experimental work of Handa.

DFT results below 100 K show a decrease in the heat capacity contribution that differs significantly from the previous behavior when compared to the ideal gas capacity. Figure 3, show different behavior below 50 K when compared to above 50 K, indicating that the hydrate backbone participates in the behavior. Additionally, the low temperature combined with the spatial restriction of the gas molecules in hydrates thanks to the backbone will force further deviation from ideality.

Thermal Expansion Coefficient. As part of our work, we computed the isobaric volumetric thermal expansion coefficient of our systems of interest, shown in Figure 5. In addition, results obtained via molecular dynamics for hexagonal ice, TMO, ethane, THF, carbon dioxide, and methane hydrates are also shown. Experimental expansion for THF hydrates and an average of sI gas hydrates are also presented. Figure 6 presents only our results to allow for closer examination of trends. It is important to note that THF hydrates, while often used as model systems for other hydrates as they can be synthesized more readily[7], are sII and not sI hydrates[35].

Figure 5 confirms the adherence to traditional solid trends for heat capacity. Since the thermal expansion coefficient is so small, the expansion contribution to constant pressure heat capacity is very low, leaving it nearly equal to the constant volume heat capacity. Figure 5 also shows that DFT vastly underestimates the thermal expansion coefficient of gas hydrates and ice when compared to the experimentally determined expansions, as well as those determined with molecular dynamics, because of the complex bonding environment present and the usage of the QHA on a relatively soft material. While using the SCAN + rVV10 functional provides accurate energies, the additional approximation and assumptions needed for the

QHA create differences in computed properties in certain bonding environments[53]. Softer materials show increased deviation for computed thermal expansion under the QHA. Diamond has a bulk modulus of 442 GPa with a maximum deviation of 9% when compared to theoretical studies and copper has a bulk modulus of 140 GPa with a maximum deviation of 36%.[54] Methane gas hydrate have bulk moduli of approximately 9 GPa[55], and the deviation with experimental results grows with temperature. One set of molecular dynamics measurements[13] shows two different trends: at low temperature, trimethyl oxide and ethane hydrate have very similar heat capacity, but as the temperature increases, the ethane hydrate has a decreasing thermal expansion. This trend goes against that which has been calculate with DFT and against the experimental value. Also, molecular dynamics studies do not display the negative thermal expansion behavior close to zero Kelvin, while experimental sI hydrates do. Two other MD studies showed expansions that carbon dioxide and methane hydrates[18] were similar to ice[56]. Experimental studies also display the same spread and variation in values for hydrate and ice thermal expansion. Therefore, we will enhance our examination by looking at just DFT results in Figure 6.

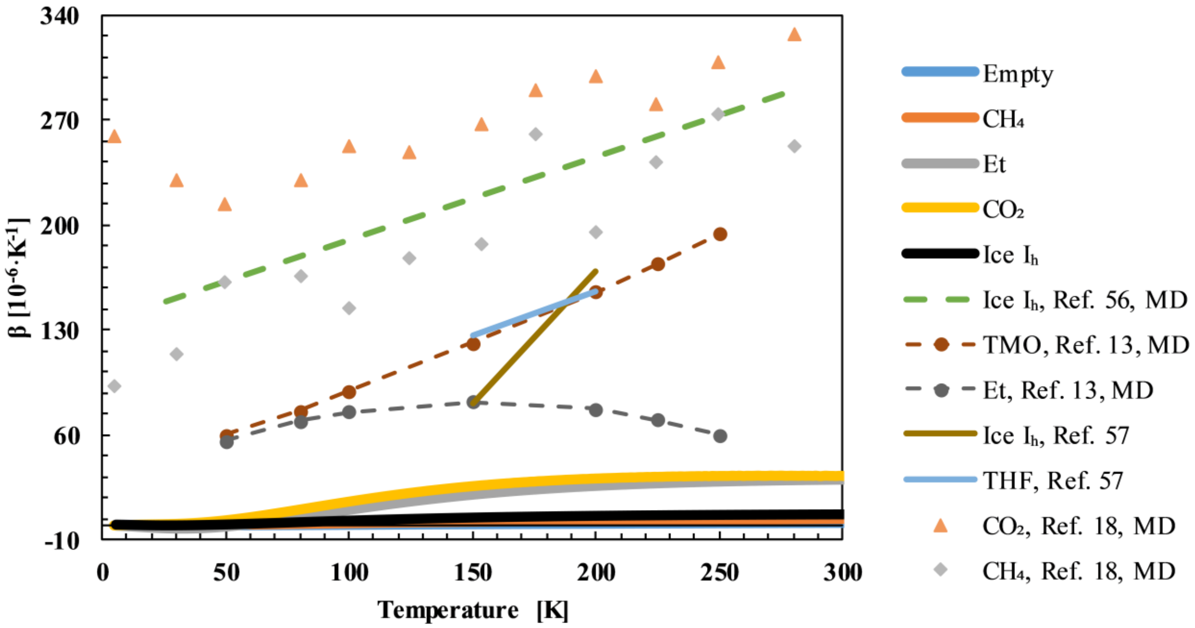

Figure 5. Temperature dependence of the isobaric volumetric thermal expansion coefficient of various sI hydrate systems and hexagonal ice. Experimental results are provided for THF hydrates and hexagonal

ice.[57] MD results are provided for hexagonal ice[56], TMO and Et sI hydrates[13], and CO_2 and CH_4 sI hydrates.[18]

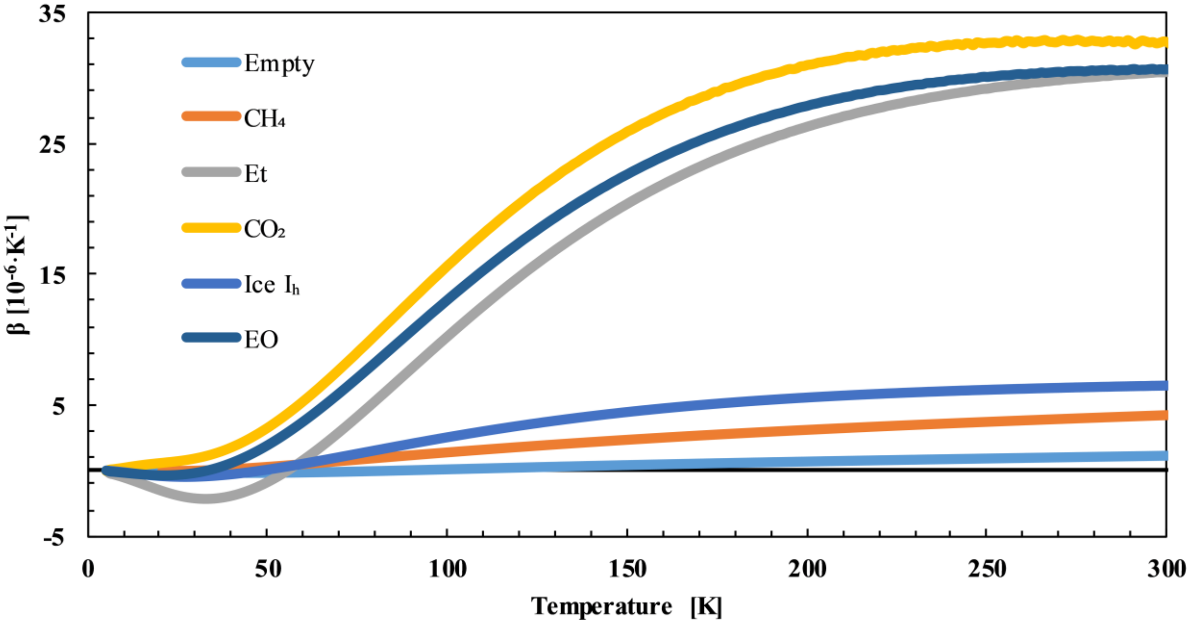

Figure 6. Temperature dependence of the isobaric volumetric thermal expansion coefficient of various sI hydrates systems and hexagonal ice calculated with DFT.

In this part of our work, a system containing EO was also added to examine the effect of polarity, specifically on thermal expansion. The calculated thermal expansion of the EO, ethane, and carbon dioxide hydrates was higher than hexagonal ice and independent of polarity, while the empty hydrates and the methane hydrate were lower than hexagonal ice beyond 50 Kelvin. This is in contrast to another DFT study, which found the thermal expansion of the carbon dioxide hydrate to be lower than that of hexagonal ice.[58] The empty and methane hydrates are much closer to ice than carbon dioxide and ethane hydrates because, structurally, they are most like ice. The methane in the hydrate is small enough that thermal expansion or contract does not constrain it and make it interact strongly with the backbone. The carbon dioxide, ethane, and EO hydrates have thermal expansions that are initially much more sensitive to temperature but plateau at 240 Kelvin. This difference is due to the equilibrium structures. We found that in the EO, carbon dioxide, and ethane hydrates, all guest molecules in the $5^{12}6^2$ cages aligned themselves parallel to the hexagonal face of the $5^{12}6^2$ cages. Those in the 5^{12} cages also were aligned with that face, but to a lesser degree. This finding confirms another DFT study that examined the CO_2 guest molecule specifically[59], and found the same alignment. Our work finds the same behavior for EO and ethane, and this interaction and subsequent deformation of the backbone cause the anomalous, when compared to the other hydrates, thermal expansion.

Figure 6 displays the negative thermal expansion at low temperatures for hexagonal ice, as well as for the empty, ethane, and methane hydrates. Experimentally, hexagonal ice has been shown to have negative thermal expansion at very low temperatures[60], but there is a lack, due to technical difficulties, of very low temperature measurements[57]. Negative thermal expansion behavior, with respect to temperature, has been shown to exist in graphene[61,62], albeit at large temperature ranges. Ceramics may also sometimes exhibit this behavior as well, although the goal for research in that field is to produce composites with specific expansions. In certain structures, heating up materials increases the bending vibrations of structures without increasing the length of the underlying bonds, decreasing the overall length of molecules or structures.[63] At low temperature, the hydrate backbone combined with guests containing smaller effective radii may allow for such behavior.

Grüneisen Parameter. We computed the Grüneisen parameter of the sI hydrate backbone, methane, ethane, EO, and CO_2 sI hydrates, and hexagonal ice as functions of temperature. Experimental values for the THF hydrate and hexagonal ice are plotted alongside our DFT results in Figure 7. The Grüneisen parameter is used to explain the effect on vibrational and thermal properties introduced by a volume change, and as such explains how temperature affects these properties by affecting volume. It is also useful to set theoretical limits on parameters and allows for the estimation of the temperature dependence of thermal properties.[64] For instance, directly measuring many thermodynamic parameters of materials within the Earth is exceptionally difficult. Determining the Grüneisen parameter allows for their estimation and to alternate between a variety of parameters.[65] Our work would allow for the determination of further properties of sI hydrates, and/or to identify materials found deep within the earth.

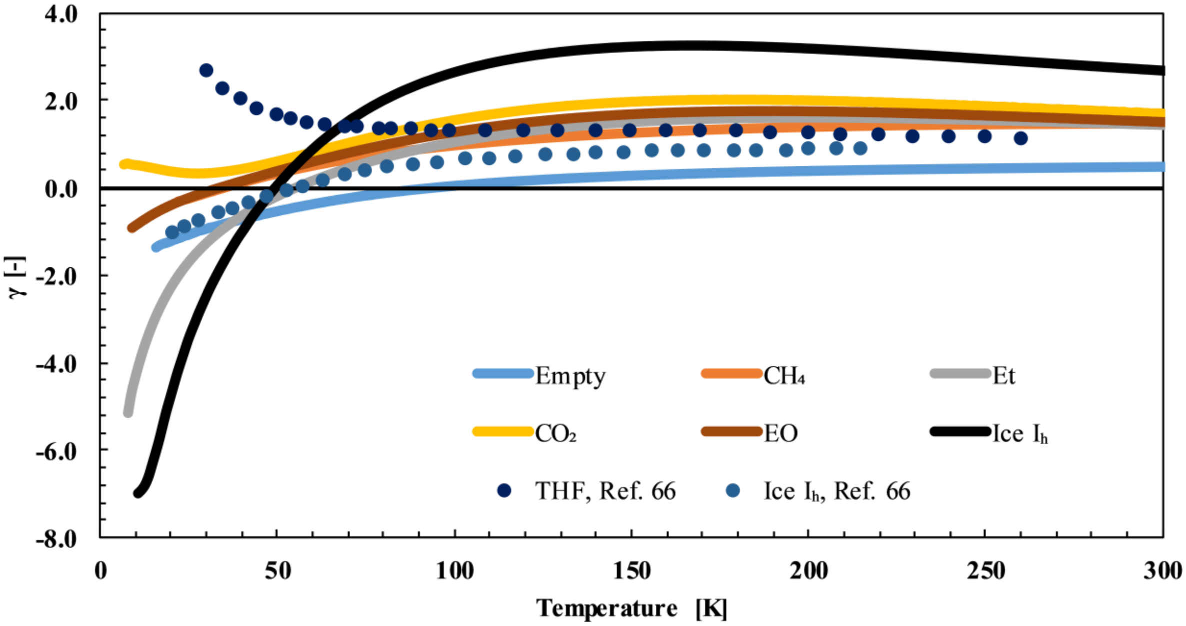

Figure 7. Temperature dependence of the Grüneisen parameter of various sI hydrate systems and hexagonal ice. Experimental results are provided for THF hydrates and hexagonal ice.[66]

Figure 7 shows the similar behavior for all sI hydrates except for the carbon dioxide hydrate. All filled hydrates approach a Grüneisen parameter of 1.7 as the temperature increases. All systems of interest in this study follow similar trends after approximately 40 Kelvin. There is a continued increase in the Grüneisen parameter followed by a plateau and approach towards a constant. The approach to a constant value is consistent with experimental data for hydrates and most materials in general[57,64]. The empty hydrate approaches a smaller value of 0.5 at 300 Kelvin. Notably, the carbon dioxide hydrate does not have a negative Grüneisen parameter. Because one of the formulations of the Grüneisen parameter is based on the thermal expansion coefficient, the exclusively positive behavior of the carbon dioxide system is tied to the exclusively positive thermal expansion coefficient of the hydrate.

Experimental values for the THF hydrate show behavior that goes against the results calculated with DFT. THF hydrates are sII hydrates, but similar trends are expected for most materials. The unusual behavior of an increasing Grüneisen parameter with decrease temperature has been seen in crystals doped with impurities as well as disordered materials[67]. However, gas hydrates are not disordered materials, due to their periodic and crystalline nature. The general trend towards a constant value is consistent with DFT, but the approach is not. The same study presents values for hexagonal ice. The Grüneisen parameter is lower experimentally beyond 40 Kelvin. The DFT gas hydrates behave more like the experimental hexagonal ice than the calculated hexagonal ice. If ice samples have impurities, they may seem to behave like hydrates because hydrates are nearly hexagonal ice containing guest molecules. The empty hydrate behaved the most closely like the experimental hexagonal ice.

CONCLUSIONS

The heat capacities, thermal expansion, and Grüneisen parameter of various sI gas hydrates presented in this work represent a significant contribution to the small database of thermal properties for these structures, undoubtably caused by experimental complexities arising at high pressure-low temperature conditions. The methodology integrates DFT simulations at 0K with phonon calculations at higher temperatures, which is a novel approach in gas hydrate research. The results provide an atomistic view into macroscopic engineering properties, clearly showing differences between the effects of guest molecules and how they interact with the hydrate backbone. A significant effort was made to compare DFT-based results with available experimental data and MD simulations. In general terms, we find that the higher fidelity afforded by DFT, results in somewhat more quantitative consistency with actual thermal property data than MD predictions. For constant volume heat capacity, DFT showed lower values for all structures when compared to MD and more consistency with experimental data. In the constant pressure heat capacity case, DFT performed very well at very low temperatures, replicating experimental results well and outperforming MD results. Hydrates and ice show little expansion contribution to the heat capacity, displacing small thermal expansion coefficients. Ethane, carbon dioxide, and ethylene oxide hydrates demonstrated behavior that was markedly different when compared to ice, methane, and the empty hydrate. The Grüneisen parameter was overestimated for filled hydrates and hexagonal ice compared to experimental results. Hydrates were found to have very similar heat capacities to ice but were all higher than ice for low temperatures. Guest molecules were shown to bring their ideal gas heat capacity to the overall system heat capacity, but additionally, through interaction with the hydrate backbone, providing more energy storage capacity to the systems. The significant signature of negative thermal expansion shown in all systems except for carbon dioxide hydrates showed that all systems showed the ice-like behavior at very low temperatures. All guest molecules except for methane displayed alignment with the $5^{12}6^2$ faces of the large cages in the hydrate, showing that there is a plane of minimum energy in the system only seen for carbon dioxide hydrates previously. This alignment manifested its effect the most in the thermal expansion coefficient, where the hydrates with these guests showed behavior that was markedly different when compared to methane hydrates, empty hydrates, and hexagonal ice. This work bridged the gap that existed at the low temperature range of the spectrum of properties, with MD unable to accurately predict the properties at such low temperatures and experiments unable to get so close to absolute zero. This work also showed that DFT, in combination with fundamental thermodynamics, can use a zero-Kelvin system as a base for higher temperature studies without needing to resort to a coarser approach for a system of this size in MD. This work presents a workflow for calculating thermal properties, using density functional theory, that allows for a high throughput of data for any original unit cell. Also, this work could present quality input data for MD simulations seeking to replicate experiments and predict properties at higher temperatures, where DFT fails. This work could be used to provide a reference for low temperature fitting of CO_2-, CH_4-, and C_2H_6-H_2O potentials to *ab initio* data. Additionally, this work provides a reference for the fit of Lennard-Jones parameters in the gas-water interaction that occurs in gas hydrates.

In future work, techniques could be developed to avoid the over-resolution of temperature effects seen in the DFT results when compared to experimental results for heat capacity. Additionally, the thermal conductivity of gas hydrates could be calculated using DFT and fundamental thermodynamics at extreme computational cost. Developing effective coarse-grained models for the hydrate could be crucial in this calculation.

ASSOCIATED CONTENT

Supporting Information

The quantities computed in this work are summarized and further defined, with their fundamental equations, and a more detailed flowchart of the calculation process is also provided.

AUTHOR INFORMATION

Corresponding Author

*E-mail: alejandro.rey@mcgill.ca.

Author Contributions

The manuscript was written through contributions of all authors. All authors have given approval to the final version of the manuscript.

ACKNOWLEDGMENT

We would like to gratefully acknowledge the support of the Natural Science and Engineering Research Council of Canada (NSERC). We would also like to acknowledge the computational resources and support provided by Compute Canada, Calcul Québec, and WestGrid. SM is thankful for scholarship support from McGill University. ADR is thankful for financial support from McGill University through the James McGill Professorship appointment.

REFERENCES

(1) Carroll, J. *Natural Gas Hydrates: A Guide for Engineers*, 3rd ed.; Gulf Professional Publishing, 2014.

(2) Cheng, C.; Wang, F.; Tian, Y.; Wu, X.; Zheng, J.; Zhang, J.; Li, L.; Yang, P.; Zhao, J. Review and Prospects of Hydrate Cold Storage Technology. *Renew. Sustain. Energy Rev.* **2020**, *117*, 109492. https://doi.org/10.1016/j.rser.2019.109492.

(3) Demirbas, A. *Methane Gas Hydrate*; Springer Science & Business Media, 2010.

(4) Yang, L.; Liu, Y.; Zhang, H.; Xiao, B.; Guo, X.; Wei, R.; Xu, L.; Sun, L.; Yu, B.; Leng, S.; Li, Y. The Status of Exploitation Techniques of Natural Gas Hydrate. *Chin. J. Chem. Eng.* **2019**, *27*, 2133–2147. https://doi.org/10.1016/j.cjche.2019.02.028.

(5) Merey, S.; Longinos, S. N. The Gas Hydrate Potential of the Eastern Mediterranean Basin. *Bull. Miner. Res. Explor.* **2019**, *160*, 117–134. https://doi.org/10.19111/bulletinofmre.502275.

(6) Sloan, E. D. Gas Hydrates: Review of Physical/Chemical Properties. *Energy Fuels* **1998**, *12*, 191–196. https://doi.org/10.1021/ef970164+.

(7) Vlasic, T. M.; Servio, P. D.; Rey, A. D. THF Hydrates as Model Systems for Natural Gas Hydrates: Comparing Their Mechanical and Vibrational Properties. *Ind. Eng. Chem. Res.* **2019**, *58*, 16588–16596. https://doi.org/10.1021/acs.iecr.9b02698.

(8) Vlasic, T. M.; Servio, P. D.; Rey, A. D. Effect of Guest Size on the Mechanical Properties and Molecular Structure of Gas Hydrates from First-Principles. *Cryst. Growth Des.* **2017**, *17*, 6407–6416. https://doi.org/10.1021/acs.cgd.7b01072.

(9) Daghash, S. M.; Servio, P.; Rey, A. D. Structural Properties of SH Hydrate: A DFT Study of Anisotropy and Equation of State. *Mol. Simul.* **2019**, *45*, 1524–1537. https://doi.org/10.1080/08927022.2019.1660326.

(10) Jendi, Z. Multiscale Modelling of Gas Hydrate Mechanical and Thermal Properties, McGill University Libraries, Montreal, 2016.

(11) Beltran, J. G.; Bruusgaard, H.; Servio, P. Gas Hydrate Phase Equilibria Measurement Techniques and Phase Rule Considerations. *J. Chem. Thermodyn.* **2012**, *44*, 1–4. https://doi.org/10.1016/j.jct.2011.08.026.

(12) Mirzaeifard, S.; Servio, P.; Rey, A. D. Multiscale Modeling and Simulation of Water and Methane Hydrate Crystal Interface. *Cryst. Growth Des.* **2019**, *19*, 5142–5151. https://doi.org/10.1021/acs.cgd.9b00578.

(13) Ghafari, H.; Mohammadi-Manesh, H. The Thermal Properties of Binary Structure SI Clathrate Hydrate from Molecular Dynamics Simulation. *Mol. Simul.* **2019**, *45*, 614–622. https://doi.org/10.1080/08927022.2019.1572142.

(14) Khokhar, A. A.; Gudmundsson, J. S.; Sloan, E. D. Gas Storage in Structure H Hydrates. *Fluid Phase Equilibria* **1998**, *150–151*, 383–392. https://doi.org/10.1016/S0378-3812(98)00338-0.

(15) Rosenbaum, E. J.; English, N. J.; Johnson, J. K.; Shaw, D. W.; Warzinski, R. P. Thermal Conductivity of Methane Hydrate from Experiment and Molecular Simulation. *J. Phys. Chem. B* **2007**, *111*, 13194–13205. https://doi.org/10.1021/jp074419o.

(16) Rosenbaum, E. J.; English, N. J.; Johnson, J. K.; Shaw, D. W.; Warzinski, R. P. Thermal Conductivity of Methane Hydrate from Experiment and Molecular Simulation. *J. Phys. Chem. B* **2007**, *111*, 13194–13205. https://doi.org/10.1021/jp074419o.

(17) Jendi, Z. M.; Servio, P.; Rey, A. D. Ab Initio Modelling of Methane Hydrate Thermophysical Properties. *Phys. Chem. Chem. Phys.* **2016**, *18*, 10320–10328. https://doi.org/10.1039/c5cp06530e.

(18) Ning, F. L.; Glavatskiy, K.; Ji, Z.; Kjelstrup, S.; Vlugt, T. J. H. Compressibility, Thermal Expansion Coefficient and Heat Capacity of CH_4 and CO_2 Hydrate Mixtures Using Molecular Dynamics Simulations. *Phys. Chem. Chem. Phys.* **2015**, *17*, 2869–2883. https://doi.org/10.1039/C4CP04212C.

(19) Kresse, G.; Furthmüller, J. Efficiency of Ab-Initio Total Energy Calculations for Metals and Semiconductors Using a Plane-Wave Basis Set. *Comput. Mater. Sci.* **1996**, *6*, 15–50. https://doi.org/10.1016/0927-0256(96)00008-0.

(20) Kresse, G.; Furthmüller, J. Efficient Iterative Schemes for Ab Initio Total-Energy Calculations Using a Plane-Wave Basis Set. *Phys. Rev. B* **1996**, *54*, 11169–11186. https://doi.org/10.1103/PhysRevB.54.11169.

(21) Kresse, G.; Hafner, J. Ab Initio Molecular-Dynamics Simulation of the Liquid-Metal-Amorphous-Semiconductor Transition in Germanium. *Phys. Rev. B* **1994**, *49*, 14251–14269. https://doi.org/10.1103/PhysRevB.49.14251.

(22) Kresse, G.; Hafner, J. Ab Initio Molecular Dynamics for Liquid Metals. *Phys. Rev. B* **1993**, *47*, 558–561. https://doi.org/10.1103/PhysRevB.47.558.

(23) Sun, J.; Ruzsinszky, A.; Perdew, J. P. Strongly Constrained and Appropriately Normed Semilocal Density Functional. *Phys. Rev. Lett.* **2015**, *115*, 036402. https://doi.org/10.1103/PhysRevLett.115.036402.

(24) Sun, J.; Remsing, R. C.; Zhang, Y.; Sun, Z.; Ruzsinszky, A.; Peng, H.; Yang, Z.; Paul, A.; Waghmare, U.; Wu, X.; Klein, M. L.; Perdew, J. P. Accurate First-Principles Structures and Energies of Diversely Bonded Systems from an Efficient Density Functional. *Nat. Chem.* **2016**, *8*, 831–836. https://doi.org/10.1038/nchem.2535.

(25) Singh, R.; Harbola, M. K. A Study of Accurate Exchange-Correlation Functionals through Adiabatic Connection. *J. Chem. Phys.* **2017**, *147*, 144105. https://doi.org/10.1063/1.4995698.

(26) Wang, R.; Carnevale, V.; Klein, M. L.; Borguet, E. First-Principles Calculation of Water PKa Using the Newly Developed SCAN Functional. *J. Phys. Chem. Lett.* **2019**, *11*, 54–59. https://doi.org/10.1021/acs.jpclett.9b02913.

(27) Dion, M.; Rydberg, H.; Schröder, E.; Langreth, D. C.; Lundqvist, B. I. Van Der Waals Density Functional for General Geometries. *Phys. Rev. Lett.* **2004**, *92*, 246401. https://doi.org/10.1103/PhysRevLett.92.246401.

(28) Román-Pérez, G.; Soler, J. M. Efficient Implementation of a van Der Waals Density Functional: Application to Double-Wall Carbon Nanotubes. *Phys. Rev. Lett.* **2009**, *103*, 096102. https://doi.org/10.1103/PhysRevLett.103.096102.

(29) Peng, H.; Yang, Z.-H.; Perdew, J. P.; Sun, J. Versatile van Der Waals Density Functional Based on a Meta-Generalized Gradient Approximation. *Phys. Rev. X* **2016**, *6*, 041005. https://doi.org/10.1103/PhysRevX.6.041005.

(30) Lee, K.; Murray, É. D.; Kong, L.; Lundqvist, B. I.; Langreth, D. C. Higher-Accuracy van Der Waals Density Functional. *Phys. Rev. B* **2010**, *82*, 081101. https://doi.org/10.1103/PhysRevB.82.081101.

(31) Blöchl, P. E. Projector Augmented-Wave Method. *Phys. Rev. B* **1994**, *50*, 17953–17979. https://doi.org/10.1103/PhysRevB.50.17953.

(32) Kresse, G.; Joubert, D. From Ultrasoft Pseudopotentials to the Projector Augmented-Wave Method. *Phys. Rev. B* **1999**, *59*, 1758–1775. https://doi.org/10.1103/PhysRevB.59.1758.

(33) PREC - Vaspwiki. Vienna Ab initio Simulation Package April 19, 2019.

(34) David S. Scholl; Janice A. Steckel. *Density Functional Theory: A Practical Introduction*; John Wiley & Sons, Inc., 2009.

(35) Sloan, E. D.; Koh, C. *Clathrate Hydrates of Natural Gases, Third Edition*; CRC Press, 2007.

(36) Takeuchi, F.; Hiratsuka, M.; Ohmura, R.; Alavi, S.; Sum, A. K.; Yasuoka, K. Water Proton Configurations in Structures I, II, and H Clathrate Hydrate Unit Cells. *J. Chem. Phys.* **2013**, *138*, 124504. https://doi.org/10.1063/1.4795499.

(37) Bernal, J. D.; Fowler, R. H. A Theory of Water and Ionic Solution, with Particular Reference to Hydrogen and Hydroxyl Ions. *J. Chem. Phys.* **1933**, *1*, 515–548. https://doi.org/10.1063/1.1749327.

(38) Momma, K.; Izumi, F. VESTA3 for Three-Dimensional Visualization of Crystal, Volumetric and Morphology Data. *J. Appl. Crystallogr.* **2011**, *44*, 1272–1276. https://doi.org/10.1107/S0021889811038970.

(39) Stukowski, A. Visualization and Analysis of Atomistic Simulation Data with OVITO–the Open Visualization Tool. *Model. Simul. Mater. Sci. Eng.* **2009**, *18*, 015012. https://doi.org/10.1088/0965-0393/18/1/015012.

(40) Togo, A.; Tanaka, I. First Principles Phonon Calculations in Materials Science. *Scr. Mater.* **2015**, *108*, 1–5. https://doi.org/10.1016/j.scriptamat.2015.07.021.

(41) Vandenberghe, W. G.; Fischetti, M. V. Calculation of Electron-Phonon Interaction Strength from First Principles in Graphene and Silicon. In *2014 International Workshop on Computational Electronics (IWCE)*; IEEE: Paris, France, 2014; pp 1–2. https://doi.org/10.1109/IWCE.2014.6865830.

(42) Yang, H.; Yang, J.; Savory, C. N.; Skelton, J. M.; Morgan, B. J.; Scanlon, D. O.; Walsh, A. Highly Anisotropic Thermal Transport in $LiCoO_2$. *J. Phys. Chem. Lett.* **2019**, *10*, 5552–5556. https://doi.org/10.1021/acs.jpclett.9b02073.

(43) Yeandel, S. R.; Molinari, M.; Parker, S. C. The Impact of Tilt Grain Boundaries on the Thermal Transport in Perovskite $SrTiO_3$ Layered Nanostructures. A Computational Study. *Nanoscale* **2018**, *10*, 15010–15022. https://doi.org/10.1039/C8NR02234H.

(44) Vlasic, T. M.; Servio, P. D.; Rey, A. D. Infrared Spectra of Gas Hydrates from First-Principles. *J. Phys. Chem. B* **2019**. https://doi.org/10.1021/acs.jpcb.8b10223.

(45) Nakagawa, R.; Hachikubo, A.; Shoji, H. Dissociation and Specific Heats of Gas Hydrate under Submarine and Sublacustrine Environments. In *Proceedings of the 6th International Conference on Gas Hydrates*; Vancouver, B.C., 2008. https://doi.org/10.14288/1.0041144.

(46) Handa, Y. P. Compositions, Enthalpies of Dissociation, and Heat Capacities in the Range 85 to 270 K for Clathrate Hydrates of Methane, Ethane, and Propane, and Enthalpy of Dissociation of Isobutane Hydrate, as Determined by a Heat-Flow Calorimeter. *J. Chem. Thermodyn.* **1986**, *18*, 915–921. https://doi.org/10.1016/0021-9614(86)90149-7.

(47) Sugisaki, M.; Suga, H.; Seki, S. Calorimetric Study of the Glassy State. IV. Heat Capacities of Glassy Water and Cubic Ice. *Bull. Chem. Soc. Jpn.* **1968**, *41*, 2591–2599. https://doi.org/10.1246/bcsj.41.2591.

(48) Tse, J. S.; Klein, M. L.; McDonald, I. R. Computer Simulation Studies of the Structure I Clathrate Hydrates of Methane, Tetrafluoromethane, Cyclopropane, and Ethylene Oxide. *J. Chem. Phys.* **1984**, *81*, 6146–6153. https://doi.org/10.1063/1.447569.

(49) Woolley, H. W. *Thermodynamic Functions for Carbon Dioxide in the Ideal Gas State*; National Bureau of Standards, 1954.

(50) McDowell, R. S.; Kruse, F. H. Thermodynamic Functions of Methane. *J. Chem. Eng. Data* **1963**, *8*, 547–548. https://doi.org/10.1021/je60019a023.

(51) Halford, J. O.; Miller, G. A. Standard Heat Capacities of Gaseous Methanol, Ethanol, Methane and Ethane at 279°K. by Thermal Conductivity. *J. Phys. Chem.* **1957**, *61*, 1536–1539. https://doi.org/10.1021/j150557a018.

(52) Gurvich, L. V.; Veyts, I. V.; Alcock, C. B. *Thermodynamic Properties of Individual Substances*, 4th Revised edition edition.; Hemisphere Pub: New York, 1989.

(53) Guan, P.-W.; Houchins, G.; Viswanathan, V. Uncertainty Quantification of DFT-Predicted Finite Temperature Thermodynamic Properties within the Debye Model. *J. Chem. Phys.* **2019**, *151*, 244702. https://doi.org/10.1063/1.5132332.

(54) Erba, A.; Shahrokhi, M.; Moradian, R.; Dovesi, R. On How Differently the Quasi-Harmonic Approximation Works for Two Isostructural Crystals: Thermal Properties of Periclase and Lime. *J. Chem. Phys.* **2015**, *142*, 044114. https://doi.org/10.1063/1.4906422.

(55) Jendi, Z. M.; Rey, A. D.; Servio, P. Ab Initio DFT Study of Structural and Mechanical Properties of Methane and Carbon Dioxide Hydrates. *Mol. Simul.* **2015**, *41*, 572–579. https://doi.org/10.1080/08927022.2014.899698.

(56) Costandy, J.; Michalis, V. K.; Tsimpanogiannis, I. N.; Stubos, A. K.; Economou, I. G. Molecular Dynamics Simulations of Pure Methane and Carbon Dioxide Hydrates: Lattice Constants and Derivative Properties. *Mol. Phys.* **2016**, *114*, 2672–2687. https://doi.org/10.1080/00268976.2016.1241442.

(57) Tse, J. S. Thermal Expansion of Structure-H Clathrate Hydrates. *J. Incl. Phenom. Mol. Recognit. Chem.* **1990**, *8*, 25–32. https://doi.org/10.1007/BF01131285.

(58) Jendi, Z.; Servio, P.; Rey, A. Ab Initio Modelling of Methane Hydrate Thermophysical Properties. *Phys Chem Chem Phys* **2016**, *18*. https://doi.org/10.1039/C5CP06530E.

(59) Izquierdo-Ruiz, F.; Otero-de-la-Roza, A.; Contreras-Garcia, J.; Prieto-Ballesteros, O.; Recio, J. M. Effects of the CO_2 Guest Molecule on the SI Clathrate Hydrate Structure. *Materials* **2016**, *9*.

(60) Yates, B. *Thermal Expansion.*; Plenum Press: New York, 1972.

(61) Yoon, D.; Son, Y.-W.; Cheong, H. Negative Thermal Expansion Coefficient of Graphene Measured by Raman Spectroscopy. *Nano Lett.* **2011**, *11*, 3227–3231. https://doi.org/10.1021/nl201488g.

(62) Mann, S.; Kumar, R.; Jindal, V. K. Negative Thermal Expansion of Pure and Doped Graphene. *RSC Adv.* **2017**, *7*, 22378–22387. https://doi.org/10.1039/C7RA01591G.

(63) Attfield, J. P. Phosphates. In *Encyclopedia of Materials: Science and Technology*; Buschow, K. H. J., Cahn, R. W., Flemings, M. C., Ilschner, B., Kramer, E. J., Mahajan, S., Veyssière, P., Eds.; Elsevier: Oxford, 2001; pp 6896–6901. https://doi.org/10.1016/B0-08-043152-6/01222-5.

(64) Vočadlo, L.; Poirer, J. P.; Price, G. Grüneisen Parameters and Isothermal Equations of State. *Am. Mineral.* **2000**, *85*. https://doi.org/10.2138/am-2000-2-319.

(65) Stacey, F. D. Applications of Thermodynamics to Fundamental Earth Physics. *Geophys. Surv.* **1977**, *3*, 175–204. https://doi.org/10.1007/BF01449192.

(66) Tse, J. S. Thermal Expansion of the Clathrate Hydrates of Ethylene Oxide and Tetrahydrofuran. *J. Phys. Colloq.* **1987**, *48*, C1-543-C1-549. https://doi.org/10.1051/jphyscol:1987174.

(67) Barron, T. H. K.; Collins, J. G.; White, G. K. Thermal Expansion of Solids at Low Temperatures. *Adv. Phys.* **1980**, *29*, 609–730. https://doi.org/10.1080/00018738000101426.

For Table of Contents Use Only

Title: Heat Capacity, Thermal Expansion Coefficient, and Grüneisen Parameter of CH_4, CO_2 and C_2H_6 Hydrates and Ice I_h via Density Functional Theory and Phonon Calculations

Authors: Samuel L. Mathews, Phillip D. Servio, Alejandro D. Rey

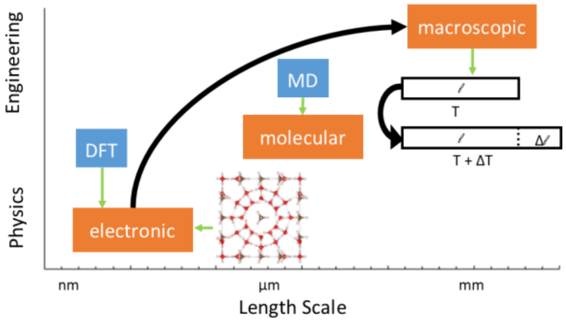

The use of computational simulation gives a molecular insight into the environmental applications of gas hydrates.